



**HAL**  
open science

# Numerical Investigation on Dynamic Ultimate Strength of Stiffened Panels Considering Real Loading Scenarios

George Jagite, Quentin Derbanne, Šime Malenica, Hervé Le Sourne, Jérôme de Lauzon, Patrice Cartraud

► **To cite this version:**

George Jagite, Quentin Derbanne, Šime Malenica, Hervé Le Sourne, Jérôme de Lauzon, et al.. Numerical Investigation on Dynamic Ultimate Strength of Stiffened Panels Considering Real Loading Scenarios. International Conference on Ships and Offshore Structures ICSOS 2018, Sep 2018, Göteborg, Sweden. pp.1-18. hal-04670916

**HAL Id: hal-04670916**

**<https://hal.science/hal-04670916v1>**

Submitted on 13 Aug 2024

**HAL** is a multi-disciplinary open access archive for the deposit and dissemination of scientific research documents, whether they are published or not. The documents may come from teaching and research institutions in France or abroad, or from public or private research centers.

L'archive ouverte pluridisciplinaire **HAL**, est destinée au dépôt et à la diffusion de documents scientifiques de niveau recherche, publiés ou non, émanant des établissements d'enseignement et de recherche français ou étrangers, des laboratoires publics ou privés.



Distributed under a Creative Commons Attribution 4.0 International License

## Numerical Investigation on Dynamic Ultimate Strength of Stiffened Panels Considering Real Loading Scenarios

George Jagite<sup>a\*</sup>, Fabien Bigot<sup>b</sup>, Quentin Derbanne<sup>b</sup>, Šime Malenica<sup>b</sup>,  
Hervé Le Sourne<sup>a</sup>, Jérôme de Lauzon<sup>b</sup>, Patrice Cartraud<sup>a</sup>

<sup>a</sup>GeM Institute UMR 6183 CNRS, Ecole Centrale Nantes, 44321 Nantes, France

<sup>b</sup>Research Department, Bureau Veritas, 92937 Paris, France

---

### Abstract

Traditionally, the hull girder ultimate strength analysis is performed under quasi-static conditions, where the maximum total vertical bending moment (VBM) of a ship, obtained from a long-term hydrodynamic analysis, is compared with the maximum VBM that the ship structure can withstand, determined from a progressive collapse analysis. In the last 10 years, the importance of whipping on the extreme hull girder loads has received much attention from designers and classification societies. The most common practice to evaluate the ultimate strength of a relatively “soft” floating structure is to compare the maximum dynamic VBM after a slamming event, which is derived from hydro-elastic calculations, with the quasi-static hull girder capacity. Some aspects regarding the current procedure remain unclear, like the capability of the current hydro-elastic methods to accurately predict the extreme dynamic response on the basis of a linear elastic structural model. Moreover, the whipping-induced stresses have a higher frequency than the ordinary wave-induced stresses; hence, the dynamic effects such as inertia and strain rate effects may provide additional strength reserves for the ship structure and should be investigated. Therefore, the aim of the research work presented in this paper was to investigate the dynamic ultimate strength of stiffened panels considering real loading scenarios, associated to wave loads and whipping response. The nonlinear finite element method was employed for a systematic analysis, in which both material and geometric nonlinearities are taken into account. Strain rate sensitivity was considered through the Cowper Symonds material model. Also, the influences of initial geometric imperfections, as well as modelling techniques were evaluated in the present study. Different combinations of in-plane biaxial loads and lateral pressure were defined to investigate the influence of dynamic effects on the ultimate capacity. The numerical results and some important insights developed from the present study are documented.

*Keywords:* dynamic capacity, ultimate strength, strain rate sensitivity, stiffened panels, whipping, ultra large container ship;

---

### 1. Introduction and motivation

Ships and offshore structures are operating in harsh ocean environment and are subjected to different physical phenomena including waves, large ship motions, slamming, spray, wind, etc. The collapse of hull girders is the most catastrophic failure event because it almost always generates the complete loss of the structure. Therefore, it is essential to ensure that the structure has sufficient strength to sustain an extreme loading situation.

Until middle of 20<sup>th</sup> century, the design criterion of ship strength was the conventional elastic bending analysis. The first attempt to evaluate the ultimate longitudinal strength of a ship's hull girder was performed by Caldwell (1965). According to Caldwell, the ultimate strength of a ship is the

---

\* Corresponding author. Tel.: +33 6 47 12 40 18  
E-mail address: george.jagite@ec-nantes.fr

bending moment which will "break the back" of the hull girder; and the real margin of safety is the difference between the ultimate bending moment and the maximum bending moment acting on the ship during its lifetime. About 10 years later, Smith (1977) proposed a simple but efficient method to perform progressive collapse analysis on a ship's hull girder in longitudinal bending by dividing the cross section into small elements composed of stiffeners and the attached plating.

In the recent years, with the increase of computer performance and developments of advanced numerical programs, it became possible to apply the finite element method (FEM) to perform collapse analysis of entire ship structures and to analyze the influence of various factors like lateral pressure, thickness reduction due to corrosion, alternate hold loading conditions, etc.

In all the procedures mentioned above, the hull girder ultimate strength analysis is performed under quasi-static conditions, where the maximum total vertical bending moment (VBM) of a ship, is compared with the maximum VBM that the ship structure can withstand, determined from a progressive collapse analysis.

However, relatively "soft" floating bodies (for example ultra large container ships) may be subjected to transient vibrations after a slamming event: an impulsive hydrodynamic impact between the hull structure and the wave. Such transient vibration of ship structure is called *whipping*. Furthermore, in the last 10 years the importance of whipping on the extreme hull girder loads has received much attention from researchers, designers and classification societies, especially after the two accidents (i.e. MSC Napoli and MOL Comfort) when the ship hull broke into two pieces after encountering severe damage of the bottom structure. The investigation reports are showing that one possible cause of the accidents is the buckling of the bottom shell plating due to hull girder loads exceeding the hull girder strength (M.A.I. 2008, ClassNK 2014).

There are several numerical methods available to analyze the slamming induced whipping response (Bishop and Price 1979, Domnisoru and Domnisoru 1998, Tuitman and Malenica 2009, Derbanne et al. 2010, Seng 2012). Recently, Andersen and Jensen (2014) performed full scale measurements on a 9400 TEU container ship showing that, due to the hull girder elasticity, the stress level is magnified by a factor of two, as presented in Fig. 1.

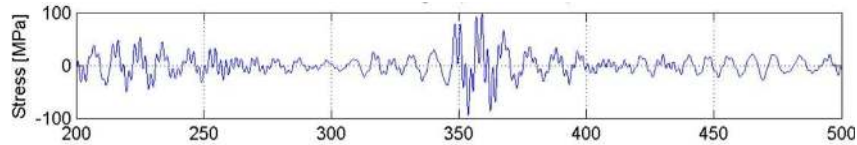


Fig. 1. Measured stress on a 9400 TEU container ship

Although it is well known that the slamming induced whipping causes a significant increase in the wave loads its consequence on hull girder's collapse is still unclear. The most common practice to evaluate the ultimate strength of a relatively "soft" floating structure is to compare the maximum dynamic VBM after a slamming event, which is derived from hydro-elastic calculations, with the quasi-static hull girder capacity. There are some uncertainties regarding the current procedure, like the capability of the current hydro-elastic methods to accurately predict the extreme dynamic response on the basis of a linear elastic structural model. Moreover, the whipping-induced stresses have a higher frequency than the ordinary wave-induced stresses; hence, the dynamic effects such as inertia and strain rate effects may provide additional strength reserves for the ship structure and should be investigated.

Several reports on the ultimate strength analysis (Amlashi and Moan 2008, Shu and Moan 2012, Matsumoto et al. 2016) showed that, at the point where the ultimate capacity is reached, only the ship's bottom panels experienced plastic deformations. Therefore, the aim of the research work presented in this paper is to analyze the dynamic effects on the ultimate strength of stiffened panels subjected to biaxial compression and lateral pressure. Since the remaining structural components are not affected by plastic deformations, the overall strain rate effect should be significantly smaller compared to one for the bottom stiffened panel.

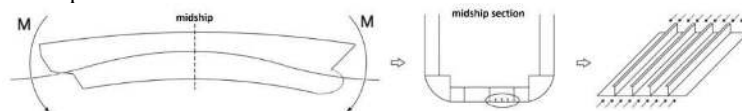


Fig. 2. Typical ship structure composition

A typical stiffened panel, as shown in Fig. 2, is composed from a thin plate and several stiffeners. It is important to note that stiffened panels are slender structures and especially vulnerable to buckling, since the predominantly loads are in-plane. Given the importance, buckling and ultimate strength of stiffened panels have been widely studied in the last century. Considering that the published literature on ultimate strength analysis of stiffened panels is overwhelming, only a short historical review together with some recent contributions are presented here.

The foundations of the linear elastic buckling theory for an ideal axial compressed column have been formulated by Euler (1759). But, the pioneering work on large deflection plate theory is attributed to Kirchoff (1850), who discovered the importance of the non-linear terms for large deformations. The final form of the plate differential equations for large deformations was derived by von Kármán (1910). Some recent work in the field of analytic or semi-analytic buckling formulations has been performed by Lin (1985), who proposed a polynomial-type empirical formula that includes two collapse modes: plate-induced and column-like collapse modes. Few years later, Paik and Kim (2002) developed a new method, based on Lin's formula, to predict the ultimate strength of stiffened panels subjected to combined axial load, in-plane bending and lateral pressure. Khedmati et al. (2010) developed closed-form formulations for predicting the ultimate strength of welded stiffened aluminum plates under combined axial in-plane loads and different levels of lateral pressure based on numerical results. Zhang (2016) developed formula for ultimate strength of steel stiffened panels in axial compression using over 100 non-linear finite element analyses.

The finite element method (FEM) was first introduced by Turner (1956), but only about 20 year later the FEM was extensively used for the analysis of stiffened plates and marine structures by Soreide et al. (1978). Nowadays, it is a normal practice in structural engineering to perform non-linear finite element analysis to assess the structural capacity of stiffened panels. Therefore, in order to obtain accurate results, few papers have been written to develop some useful insights on nonlinear finite element method application for the ultimate limit state assessment of stiffened panels (Paik and Seo 2009a,b, Zhang and Jiang 2014).

Though many experiments and numerical analyses to estimate the ultimate strength of stiffened panels have been reported, relatively little work has addressed the dynamic collapse of stiffened panels due to whipping. Jiang et al. (2012) performed verifications of the dynamic buckling analysis to investigate the influence of various factors on the ultimate strength of ship structures subjected to whipping. However, the definition of the dynamic ultimate capacity of the stiffened panel that they used seems inconsistent. To the author's knowledge, there is no comprehensive study of the dynamic effects on the ultimate strength of stiffened panels. Therefore, this paper proposes a new definition of the dynamic ultimate capacity, and presents systematic non-linear finite element analyses of the dynamic effects, i.e. strain rate and inertia, on the ultimate strength of sixteen stiffened panels subjected to bi-axial compression and lateral pressure. First, the quasi-static ultimate strength is calculated for each panel. Finally, the dynamic load factors (the ratio between the dynamic ultimate strength and the quasi-static ultimate strength) are determined for different scenarios, as well as the ratio between the whipping scenario and wave scenario load factors in order to determine how a stiffened panel capacity will be affected by whipping response.

#### Nomenclature

$a$	spacing between transverse frames
$b$	spacing between longitudinal stiffeners
$t$	plate thickness
$\beta$	plate slenderness ratio
$\lambda$	column slenderness ratio
$\sigma_0$	static yield stress
$\sigma_d$	dynamic yield stress
$CF_0$	quasi-static ultimate strength
$CF_{max}$	dynamic ultimate strength
$\bar{f}_d$	dynamic load factor increase rate
$\bar{f}_{WWR}$	whipping-wave dynamic load ratio increase rate
$\dot{\epsilon}$	strain rate

## 2. Numerical data

### 2.1. Geometry

The numerical models are based on the stiffened panels from the bottom plating of sixteen different container ships. As indicated in Fig. 3, the spacing between adjacent transverse frames is denoted by  $a$ , and the distance between adjacent longitudinal stiffeners is denoted by  $b$ . To determine the maximum capacity of a stiffened panel, the model is extending over  $\frac{1}{2}+2+\frac{1}{2}$  frame spacings in the longitudinal direction and five stiffeners in the transverse direction.

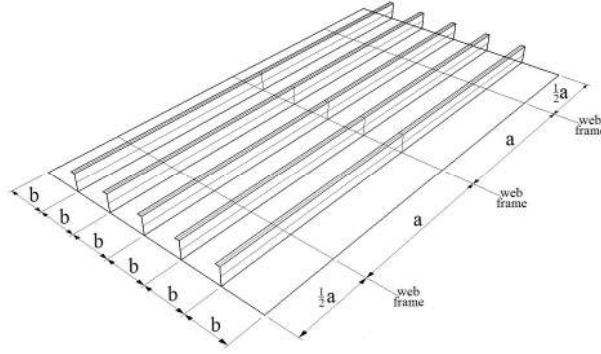


Fig. 3. Stiffened panel model extension

The dimensions of these panels and the scantlings of the stiffeners are summarized in Table 1. The plate slenderness ratio, denoted as  $\beta$ , is calculated using Eq. 1 where  $t$  represents the plate thickness,  $\sigma_0$  represents the material yield stress and  $E$  represents the material Young's modulus. The column slenderness of the beam column element (stiffener and associated plate), denoted as  $\lambda$ , is calculated using Eq. 1 where  $r$  represents the gyration radius of the stiffener with its attached plating.

$$\beta = \frac{b}{t} \cdot \sqrt{\frac{\sigma_0}{E}} \quad , \quad \lambda = \frac{a}{r} \cdot \sqrt{\frac{\sigma_0}{E}} \quad (1)$$

Table 1. Geometric characteristics of the stiffened panels considered in the present study

no	name	span [mm]	spacing [mm]	thk. [mm]	stiffener [mm]	material	$\beta$	$\lambda$
1	ia841t225	3264	841	22.5	L400x100x11.5/16	AH32	1.462	0.320
2	tb840t20	3250	840	20.0	T400x150x11/18	AH32	1.369	0.267
3	tb840t27	3250	840	27.0	T425x150x11/18	AH32	1.217	0.269
4	ia840t215	3250	840	21.5	L350x100x12/17	AH32	1.776	0.359
5	ia840t185	3250	840	18.5	L350x100x12/17	AH32	1.529	0.346
6	tb840t24	3250	840	24.0	T400x150x11/18	AH32	1.643	0.278
7	fb910t26	1625	910	26.0	FB225x21	AH32	1.369	0.371
8	ia840t145	3200	840	14.5	L250x90x12/16	AH32	2.266	0.476
9	ia860t13	3160	860	13.0	L250x90x10/15	AH32	2.588	0.463
10	ia871t155	3150	871	15.5	L300x90x11/16	AH32	2.198	0.397
11	ia875t16	3300	875	16.0	L300x90x11/16	AH32	2.139	0.420
12	ia890t20	3150	890	20.0	L350x100x12/17	AH32	1.740	0.347
13	ia910t22	2100	910	22.0	L250x90x10/15	AH32	1.618	0.296
14	tb840t24b	4200	840	24.0	T400x150x11.5/25	AH36	1.453	0.351
15	ia732t28	2100	732	28.0	L250x90x12/16	AH36	1.085	0.376
16	bb905t18	3445	905	18.0	HP260x11	AH36	2.088	0.678

## 2.2. Material properties

It is well known that the dynamic load effects can induce changes in the material strength properties, and many researchers shown that the plastic flow of some materials is sensitive to strain rate (Manjoine 1945, Cowper and Symonds 1957, Rolfe et al. 1974, Jones 2011). The Cowper Symonds constitutive model, shown in Eq. 2, is used extensively in numerical studies.

$$\frac{\sigma_d}{\sigma_0} = 1 + \left(\frac{\dot{\epsilon}}{C}\right)^{1/q} \quad (2)$$

Paik et al. (2017) developed a new test database of the mechanical properties of materials for marine applications, including mild steel and high tensile steel. The test database covers strain rates between  $10^{-3}$  and  $10^2 s^{-1}$ , and different temperatures. The new experimental results for the dynamic yield stress ratio are in very good agreement with the Cowper-Symonds constitutive equation if the constants proposed by Paik and Chung (1999) and Jones (2011) are used. It should be noted that in the tests of Paik et al. (2017) the static yield stress was determined for a strain rate of  $10^{-3} s^{-1}$ , which does not correspond with the recommendations of international standards. According to the classification societies rules (Bureau Veritas 2018, Det Norske Veritas 2018), for the determination of the upper yield stress,  $R_{eH}$ , the test shall be carried out with an elastic stress rate between 6 and 60  $MPa s^{-1}$ . On the other hand, in order to minimize the measurement uncertainty, ISO (2009) proposed a different method to be used when the strain rate sensitive parameters are analyzed. For determination of the upper yield stress,  $R_{eH}$ , the strain rate shall be kept as constant as possible, between  $7 \cdot 10^{-5}$  and  $2.5 \cdot 10^{-4} s^{-1}$ . Fig. 4 summarizes the experimental results reported by several researchers for the dynamic yield stress ratio of the high tensile steel.

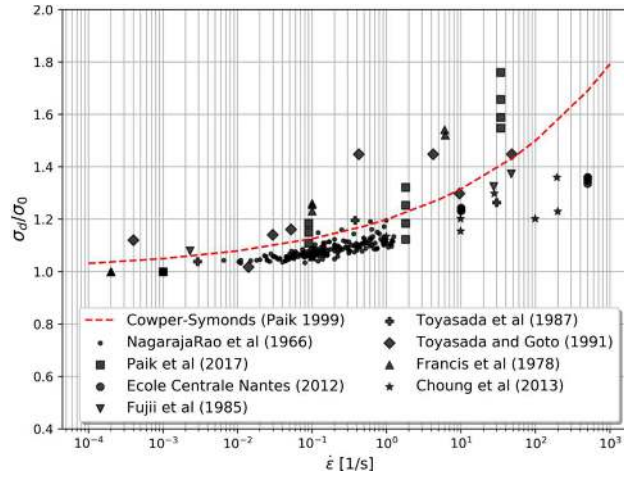


Fig. 4. Dynamic yield stress ratio for high tensile steel

In the numerical analysis, the material of the stiffened panels is high tensile steel (AH32 and AH36) with Young's modulus of 205.8  $GPa$ , Poisson ratio of 0.3 and a yield stress of 315  $MPa$ , and respectively 355  $MPa$ . Firstly, for the quasi-static analysis it is defined as an elastic-plastic material including strain hardening with a slope of 1/1000. Finally, in order to analyze the strain rate effect on the dynamic ultimate strength the following constants:  $C = 3200$ ,  $q = 5$  were used for the Cowper-Symonds constitutive material model, presented in Eq. 2. It is important to notice that according to this model, the flow stress is already increased by 3% at strain rates as low as  $10^{-4} s^{-1}$ , i.e. strain rates that are reached during “quasi-static” experiments. The effect of this “inconsistency” on the estimation of panels’ capacity will be discussed later in this paper.

## 2.3. Load cases

A systematic non-linear finite element analysis has been carried out to study the dynamic effects on the ultimate strength of stiffened panels. For each panel, six load cases of combined compressive

longitudinal stress  $\sigma_x$  and transverse stress  $\sigma_y$  are defined. Table 2 summarizes all load cases applied to the panel. For each load case, four different levels of lateral pressure are applied: 0.0, 0.1, 0.2 and respectively 0.3 MPa. Stress ratio, denoted as  $SR$  is calculated as the ratio between the axial stress and the sum of axial and transversal stresses.

Table 2. Load cases

load case	1	2	3	4	5	6
name	a1	a09t01	a07t03	a05t05	a03t07	t1
$\sigma_x$	1.0	0.9	0.7	0.5	0.3	0.0
$\sigma_y$	0.0	0.1	0.3	0.5	0.7	1.0
$SR$	1.0	0.9	0.7	0.5	0.3	0.0

#### 2.4. Boundary conditions

The choice of the boundary conditions is crucial for the accuracy of the numerical results. Therefore, in the analysis of the ultimate capacity of a stiffened panel, the following boundary conditions are adopted.

The primary supporting members (i.e. web frames) are idealized and modeled by boundary conditions. At the intersection lines between the plate and the primary supporting members, the translations on  $Z$ -axis are fixed. Also, constrain equations are applied at the intersection between stiffener webs and primary supporting members to remain vertical.

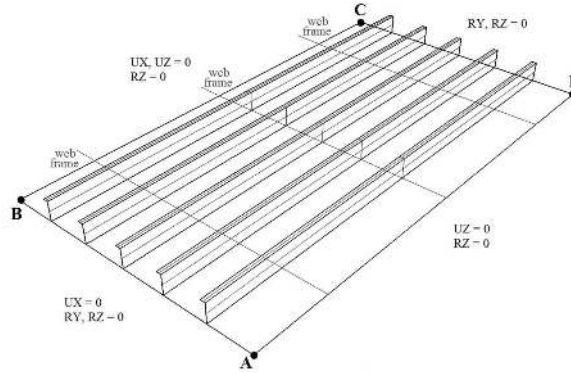


Fig. 5. Illustration where the boundary conditions are applied

In Fig. 5, the constraints imposed on the boundaries of the stiffened panel are presented. Where  $UX$ ,  $UY$  and  $UZ$  denotes the translations along  $X$ ,  $Y$  and  $Z$  axes. Similar,  $RX$ ,  $RY$  and  $RZ$  denotes the rotations around  $X$ ,  $Y$  and  $Z$  axes. Finally, the nodes on  $CD$  are constrained by equations to follow the same translation on  $X$ -axis as node  $C$ . Similar constrains are imposed for the nodes on  $AD$  to follow the same translation on  $Y$ -axis as node  $A$ . Thus, the loads will be applied as concentrated forces on nodes  $A$  and  $C$  to generate various in-plane bi-axial loads.

### 3. Numerical analyses

#### 3.1. Definition of the dynamic ultimate capacity

Finite element analyses using the computer code ABAQUS (2017) were employed in this study, in which both material and geometric nonlinearities are taken into account. In order to determine the quasi-static capacity, i.e. without any dynamic effects taken into account, the arc-length method is used. This method allows the load to be automatically increased until the ultimate capacity is reached and automatically decreased during the collapse process. If the panel is subjected to lateral pressure and combined in-plane loads then the loads are applied in two consecutive steps. In the first step the lateral pressure is applied and kept constant over the second step when the bi-axial compression is applied.

In the arc-length procedure, the load proportionally factor (*LPF*) represents one additional degree of freedom in the analysis, therefore it is not possible to use this procedure when analyzing the dynamic effects. A dynamic solver must be used for the analysis of strain rate and inertia effect. Thus, the applied loads are defined as a function of time, using a half-sine loading function described by Eq. 3, where  $T$  represents the period of the load and  $CF$  is the amplitude of the load.

$$f(t) = CF \cdot \sin\left(\frac{2\pi}{T} \cdot t\right) \quad (3)$$

Two different scenarios are considered to study the influence of the load period on the panel capacity:

- *wave period* scenario, with  $T = 8s$ ;
- *whipping period* scenario, with  $T = 1.6s$ .

It should also be mentioned that, at the scale of the entire ship, whipping is not a load but the structural response to an impulsive load. However, in the case of a stiffened panel, whipping will be considered as a periodic load imposed by the surrounding structure.

Similar loading scenarios, associated with whipping, are considered by Jiang et al. (2012) to analyze the ultimate capacity of a stiffened panel under uniform axial loads. In the study of Jiang et al., the applied load in the nonlinear dynamic analysis was defined as the quasi-static capacity  $CF_0$  multiplied by a factor of 1.2. By scaling the quasi-static capacity by a factor of 1.2, they created a load scenario in which the panel collapsed, and they observed that during the dynamic collapse the applied load gets higher than the panel static capacity. In their work, the dynamic capacity represents the applied load,  $f(t_{ib})$ , at the instant:  $t_{ib}$  when the axial displacement started to accelerate rapidly. This time point is defined as “initiation of buckling”. Since the definition based on the rapid acceleration of axial displacement is quite arbitrary and interpretable, a new definition for the “initiation of buckling” point is proposed in this paper. Therefore, the failure point of a structure subjected to a load equal to  $1.2 \cdot CF_0$  is determined as the point where the slope of the axial displacement vs. time curve is ten times bigger than the initial slope.

According to Jiang et al., the definition of the dynamic capacity and of the capacity increase is thus as follows:

$$f_{d_{ib}} = \frac{f(t_{ib})}{CF_0} = 1.2 \cdot \sin\left(\frac{2\pi}{T} \cdot t_{ib}\right) \quad , \quad \bar{f}_{d_{ib}} = 1.2 \cdot \sin\left(\frac{2\pi}{T} \cdot t_{ib}\right) - 1 \quad (4)$$

We consider that this is not a proper definition of the panel dynamic capacity. Indeed, this increased load was reached only during the panel collapse, it is a load level that the panel cannot sustain without collapsing and thus it is of very limited interest for the designer.

In this work, we consider that the proper definition of the dynamic capacity is the maximum load that can be applied on the panel without a panel collapse. Therefore, in order to determine the maximum capacity of a stiffened panel, an iterative procedure is employed in this study. Starting from  $CF = CF_0$ , the amplitude of the load ( $CF$ ) is increased until the panel fails. The panel dynamic capacity is  $CF_{max}$ : the maximum value of  $CF$  that the panel can withstand. Since we are interested in the modification of the panel capacity, we define the dynamic load factor  $f_d$  as follows:

$$f_d = \frac{CF_{max}}{CF_0} \quad , \quad \bar{f}_d = \frac{CF_{max} - CF_0}{CF_0} \quad (5)$$

Moreover, for the comparison of the dynamic load factors obtained in the whipping period and wave period scenarios, we introduce the following ratio:

$$f_{WWR} = \frac{f_{d_{whipping}}}{f_{d_{wave}}} \quad , \quad \bar{f}_{WWR} = \frac{f_{d_{whipping}} - f_{d_{wave}}}{f_{d_{wave}}} \quad (6)$$



In a static simulation, the maximum load is clearly defined, since no static equilibrium can be found when this load is exceeded. However in a dynamic simulation the load can theoretically be arbitrarily increased, the excess of load leading to an acceleration of the structure associated with very high distortion. In this work, the panel was considered has collapsed when the structural deformations become very large, with a rapid reduction in stiffness and the loss of structural stability.

### 3.2. Mesh sensitivity

It is essential to quantify the uncertainties in the numerical model, and thus a mesh convergence study is carried out. Table 3 summarizes the average mesh size and number of elements on plate (between stiffeners), stiffener web and stiffener flange. The aspect ratio of each element was kept within the range 1:1 to 1:2. The element of choice in this work is S4: a general shell element with 4 nodes, which can be used for both thin and thick shells as well as small and large strain applications.

Table 3. Mesh density

mesh size	el on span	el on spacing	el on stiffener height	el on stiffener flange
coarse	16	4	2	1
medium	32	8	4	1
fine	32	12	6	1

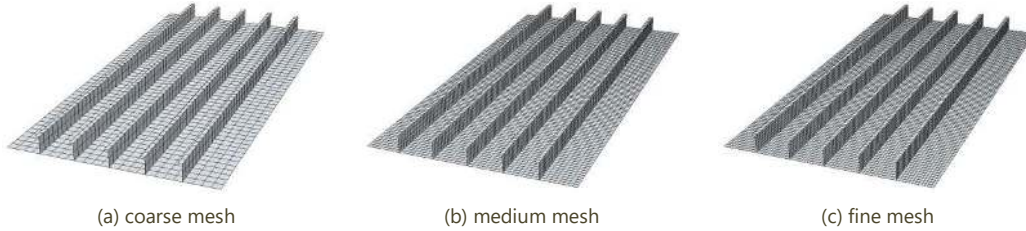


Fig. 6. Mesh distribution

The results of the sensitivity study on mesh sizes, obtained for model *ia841t225*, are presented in Table 4, where the relative difference is computed with regard to medium mesh size.

Table 4. Mesh sensitivity results

mesh size	$CF_0$ [MN]	diff [%]	$\bar{f}_{d_{wave}}$ [%]
coarse	43.133	1.95	4.6
medium	42.276	-	4.5
fine	42.143	-0.31	4.5

Judging from these results, the effect of mesh size over the dynamic load factor is negligible. However, there is a small influence over the quasi-static ultimate capacity, therefore in the following analyses the FE model with medium mesh size is used.

### 3.3. Geometric initial imperfections

A typical steel structure is usually fabricated by flame cutting and welding, and thus initial imperfections may appear and will reduce the structural capacity. These initial imperfections may be classified in initial distortions and residual stresses. Only initial imperfections related to initial distortions will be considered in this study. Several researchers reported on the importance of the geometric initial imperfections for buckling and ultimate strength analysis. According to Paik (2018), there are two ways to define the initial imperfections shape in a numerical analysis:

- the shape of the geometric initial imperfections is represented by the fundamental buckling mode for each case of biaxial compression;
- the shape of the geometric initial imperfections is represented by the fundamental buckling mode obtained for pure longitudinal compression.

An alternative method to the buckling analysis is to define the shape of initial imperfections is the use of analytical expressions and the nodal translation approach Paik (2018). Therefore, the number of half-waves in longitudinal direction, denoted as  $n_{hw}$ , for a plate subjected to biaxial compression is determined as the smallest integer value that satisfies Eq. 6:

$$\frac{(n_{hw}^2/a^2 + 1/b^2)^2}{n_{hw}^2/a^2 + c/b^2} \leq \frac{((n_{hw} + 1)^2/a^2 + 1/b^2)^2}{(n_{hw} + 1)^2/a^2 + c/b^2} \quad (6)$$

where  $c$  represents the ratio between the transverse compression  $\sigma_y$  and the longitudinal compression,  $\sigma_x$ .

After choosing the shape of the initial geometric imperfections, the next step is to define the maximum amplitude of the initial imperfections. In the current industry practice, an average magnitude for the initial imperfections is usually considered; assuming that the maximum amplitude is a function only of the distance between stiffeners, as shown in Eq. 7.

$$w_{pl} = 0.005 \cdot b \quad (7)$$

Smith et al. (1988) proposed three different levels for the maximum amplitude of the initial geometrical imperfections, as a function of plate slenderness ratio, plate thickness and a coefficient, denoted as  $c_A$ , obtained from statistical analysis, as shown in Eq. 8.

$$w_{pl} = c_A \beta^2 t \quad \text{and} \quad c_A = \begin{cases} 0.025 & \text{for a slight level} \\ 0.1 & \text{for an average level} \\ 0.3 & \text{for a severe level} \end{cases} \quad (8)$$

A sensitivity study regarding the amplitude of the initial geometric imperfections is performed, and the results obtained for model *tb840t20* are summarized in Table 5 for a stiffened panel subjected to axial compression and lateral pressure.

Table 5. Effect of the initial imperfections amplitude on the dynamic ultimate strength

initial imperfection	press. [MPa]	$CF_0$ [MN]	$\bar{f}_{d_{wave}}$	$\bar{f}_{d_{whipping}}$	$\bar{f}_{WWR}$
average	0.0	38.776	4.3%	5.8%	1.4%
	0.2	36.016	5.3%	7.1%	1.7%
slight level (Smith 1998)	0.0	42.045	4.0%	5.4%	1.3%
	0.2	38.954	5.1%	6.9%	1.7%
average level (Smith 1998)	0.0	39.126	4.2%	5.6%	1.3%
	0.2	36.347	5.2%	7.0%	1.7%
severe level (Smith 1998)	0.0	35.170	5.0%	6.9%	1.8%
	0.2	32.901	5.8%	7.8%	1.8%

The numerical results are showing that the quasi-static ultimate strength is decreasing when the initial imperfections amplitude increases. Also, the dynamic load factors for wave scenario and whipping scenario are proportionally increased with the increase of the initial imperfections amplitude. So the ratio between the dynamic load factors for whipping and wave scenarios is not significantly influenced by the initial imperfections amplitude. Therefore, in the current study the initial imperfections amplitude is taken as per the industry practice. The imperfections are generated as a combination of:

- local imperfection obtained from a linear buckling analysis. The fundamental buckling mode is retained and scaled so that the deflection of the plate is equal to  $1/200$  of the stiffeners spacing. Fig. 7a shows the local imperfection with a 250 magnification factor;

- global imperfection defined analytically, corresponding to column buckling of the plate, with a deflection equal to  $1/1000$  of the stiffeners span. Fig. 7b shows the global imperfection magnified with a factor of 100;
- global imperfection defined analytically, corresponding to torsional buckling of the stiffeners, with a deflection equal to  $1/1000$  of the stiffeners span. Fig. 7c shows the global imperfection magnified with a factor of 100.

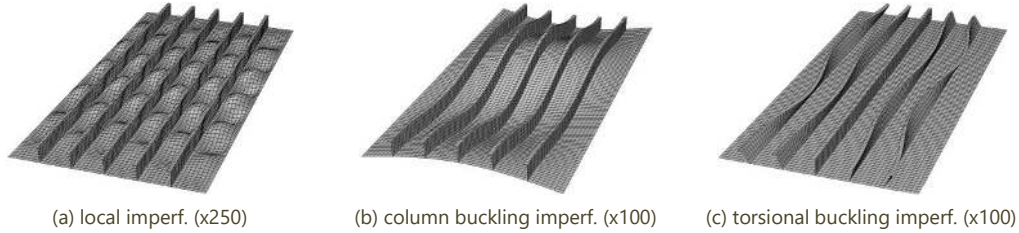


Fig. 7. Initial geometric imperfections

#### 4. Results and discussions

Prior to the nonlinear dynamic analyses, the first step was to analyze the quasi-static collapse behavior of the stiffened panels under combined in-plane compression and lateral pressure. The typical deformed shapes are presented in Fig. 8, showing that the panel failed due to plastic deformations of the attached plate.

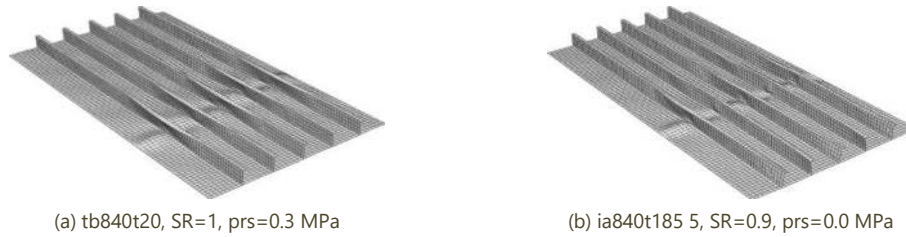


Fig. 8. Typical collapse mode of a stiffened panel

##### 4.1. Inertia effect

One purpose of this study was to investigate the influence of the inertial effect. To this effect, in a first step, the strain rate effect was excluded from the analysis by using a simple bi-linear plasticity model. The numerical results are indicating that the inertial effect on the ultimate strength of a stiffened panel is negligible for a load period varying from 1.6 to 16s. On the other hand, if the duration of the dynamic loading applied to the stiffened panel is very small, the inertia effect will slightly increase the panel's capacity, as shown in Fig. 9. For a load with a period of  $0.2\text{ s}$  the dynamic ultimate strength is increased with less than  $1\%$ .

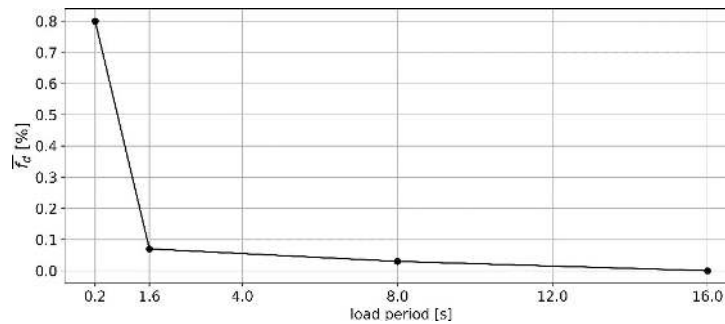


Fig. 9. Dynamic load factor vs. load period

#### 4.2. Strain rate effect

After analyzing the inertial effect on the ultimate strength, the next step is to study the influence of the strain rate on the ultimate capacity using a series of dynamic analyses. Therefore, starting from the quasi-static capacity of the stiffened panels, the dynamic capacity for each panel was determined by increasing the load amplitude until the panel fails. A typical example for the variation of the dynamic load factor under all scenarios and different load combinations is presented in Fig. 10. Similar results were obtained for all other models analyzed in this research work.

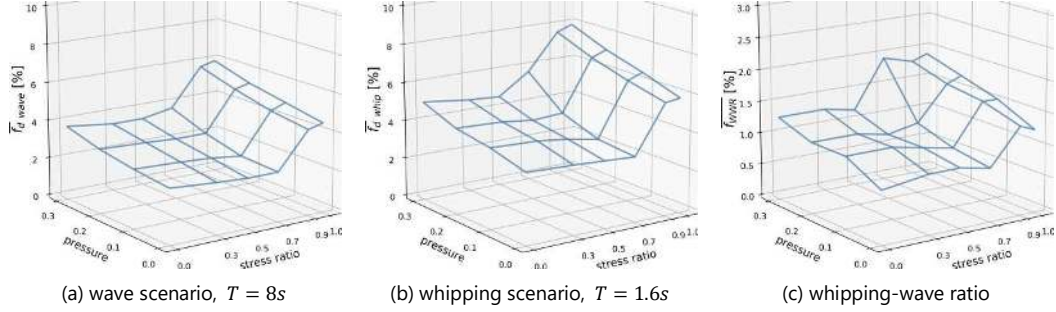


Fig. 10. Typical dynamic load factor distribution

By examining the results from the nonlinear dynamic analyses it can be concluded that the dynamic load factor increases when the load period decreases and also when the applied lateral pressure increases. Also, it can be concluded that the highest values of the dynamic load factor are obtained for pure axial compression,  $SR = 1$ . Therefore, in the following comparison only the worst load case will be considered for each stiffened panel.

In order to show the importance of correctly evaluating the dynamic ultimate strength, a comparison between the dynamic load factors obtained for the whipping period scenario using Jiang's definition (Eq. 4) on one hand, and using our new definition (Eq. 5) on the other hand was made and it is presented hereafter.

Table 8. Comparison of the different definitions of the dynamic capacity increase, for whipping scenario

model	$CF_0$ [MN]	$t_{ib}$ [s]	$\bar{f}_{d_{ib}}$	$\bar{f}_{d_{whip}}$	model	$CF_0$ [MN]	$t_{ib}$ [s]	$\bar{f}_{d_{ib}}$	$\bar{f}_{d_{whip}}$
ia840t185	34.10	0.292	9.4	5.6	ia732t28	50.43	0.298	10.5	7.2
ia840t215	40.04	0.295	9.9	5.8	ia860t13	19.81	0.294	9.8	5.2
ia841t225	42.28	0.295	9.9	6.1	ia871t155	26.20	0.290	9.0	5.2
fb910t26	48.75	0.294	9.8	6.1	ia875t16	27.37	0.289	8.8	5.0
ia840t145	23.80	0.289	8.8	4.8	ia890t20	37.50	0.292	9.4	5.4
ia910t22	36.67	0.297	10.3	5.8	tb840t24	46.75	0.295	9.9	6.2
tb840t20	38.78	0.294	9.8	5.7	tb840t24b	53.68	0.298	10.5	6.0
tb840t27	52.77	0.296	10.1	6.5	bb905t18	32.33	0.290	9.0	5.0

The numerical results presented in Table 8, when stiffened panel's structure is subjected to a load equal to  $1.2 \cdot CF_0$ , are showing that the dynamic effects will increase the dynamic capacity at the initiation of buckling from 8.8% to 10.5%. However, with the correct definition of the dynamic ultimate strength, the dynamic capacity is increased only with 4.8% to 7.2%. It can be observed that the whipping dynamic capacity increase with our definition is systematically lower than the one with Jiang's definition. The corollary is that none of the panel can actually withstand the load defined by Jiang's definition. This clearly confirms the need for the new definition.

The results of the dynamic analyses for all panels under axial compression are summarized in Table 9. In Fig. 11 we show a comparison between the dynamic load factors obtained with our new definition for wave and whipping period scenarios, together with those obtained with Jiang's definition for whipping period.

Table 9. Dynamic load factors [%] variation for axial compression

model	prs	$\bar{f}_{d_{wave}}$	$\bar{f}_{d_{whip}}$	$\bar{f}_{WWR}$	model	prs	$\bar{f}_{d_{wave}}$	$\bar{f}_{d_{whip}}$	$\bar{f}_{WWR}$
ia840t185	0.0	4.2	5.6	1.3	ia732t28	0.0	5.4	7.2	1.7
	0.25	5.4	7.2	1.7		0.3	6.1	8.3	2.1
ia840t215	0.0	4.5	5.8	1.2	ia860t13	0.0	3.8	5.2	1.3
	0.3	5.9	7.9	1.9		0.1	4.9	6.8	1.8
ia841t225	0.0	4.6	6.1	1.4	ia871t155	0.0	3.8	5.2	1.3
	0.3	5.8	7.9	2.0		0.1	4.3	6.0	1.6
fb910t26	0.0	4.5	6.1	1.5	ia875t16	0.0	3.8	5.0	1.2
	0.3	5.2	7.0	1.7		0.1	4.3	6.0	1.6
ia840t145	0.0	3.5	4.8	1.3	ia890t20	0.0	4.0	5.4	1.3
	0.3	4.3	6.0	1.6		0.2	5.0	6.8	1.7
ia910t22	0.0	4.4	5.8	1.3	tb840t24	0.0	4.6	6.2	1.5
	0.3	5.5	7.4	1.8		0.3	5.9	7.8	1.8
tb840t20	0.0	4.3	5.7	1.3	tb840t24b	0.0	4.6	6.0	1.3
	0.3	5.6	7.6	1.9		0.3	5.9	8.1	2.1
tb840t27	0.0	4.8	6.5	1.6	bb905t18	0.0	3.6	5.0	1.4
	0.3	5.9	8.0	2.0		0.2	4.9	6.7	1.7

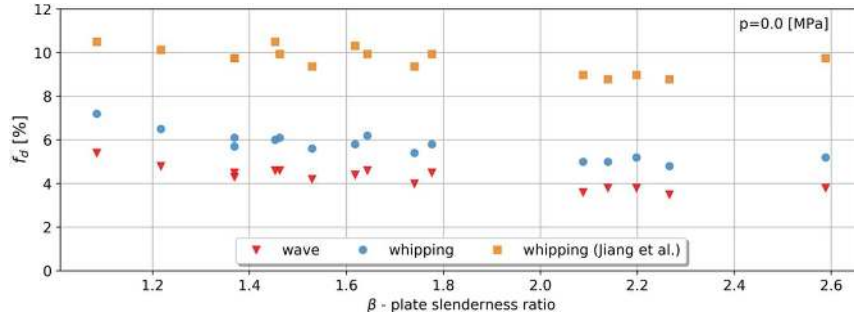


Fig. 11. Dynamic load factor for all panels under pure in-plane axial compression vs. their plane slenderness ratio

From the results shown in Table 9 and Fig 11, we can observe that the effect of strain rate is already existent for the wave period scenarios. This is not surprising since as mentioned in section 2.2, with the considered Cowper-Symonds model it was expected that some strain rate effects are observed in the response to “quasi-static” loads. However, this is in contradiction with the long established industry practice to consider the wave periods as quasi-static.

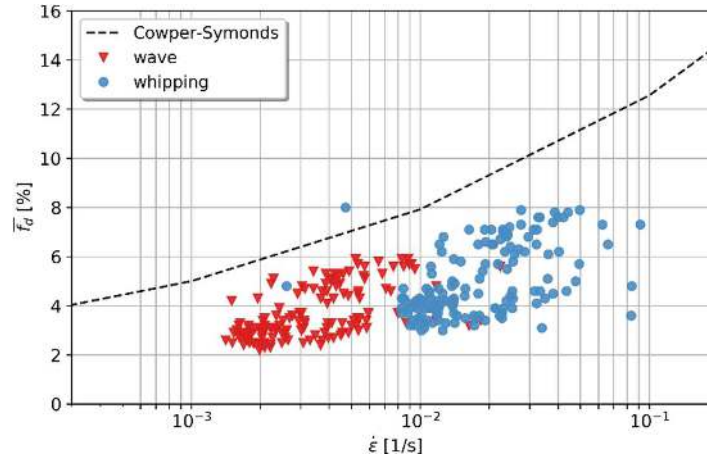


Fig. 12. Dynamic load factor vs. strain rate

We believe that two different interpretations can be made of this finding. The first interpretation is that this apparent increased capacity in the response to the wave scenario is an artefact of the considered strain rate model, and of the inconsistency mentioned in section 2.2. As a consequence, the industry practice would be confirmed, and we should change the Cowper-Symonds equation, or define another equation that would give no increase for strain rates below  $10^{-3}$  and thus no (or negligible) increased capacity for wave period scenarios.

Fig. 12 shows the dependency of the dynamic load factor with the maximum local strain rate obtained during the analysis. The numerical results are indicating that a wave scenario produces strain rates up to  $10^{-2} s^{-1}$ . On the other hand, during the whipping period scenario the strain rates are about one order of magnitude higher, in a range from about  $10^{-2} s^{-1}$  to  $10^{-1} s^{-1}$ .

These results show that the part of the Cowper-Symonds constitutive model involved in the wave period scenarios and also in the whipping period scenarios is the part where the validity of the model is questionable, as discussed in section 2.2. As shown in Fig. 13 the Cowper-Symonds curve is not very consistent with the results of the “quasi-static yield stress experiments”. By construction, the curve is significantly above the experimental data in this range of strain rates. The only exceptions are a few experimental points for which it is not clear how the “quasi-static” yield stress used to normalize the data has been defined, since these points are far above 1.0 at very low strain rates.

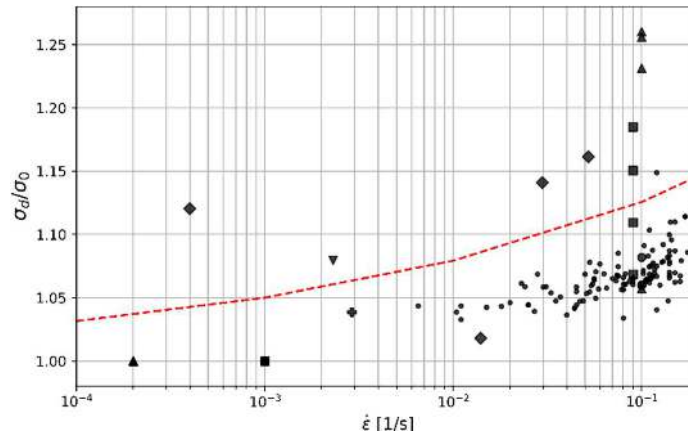


Fig. 13. Dynamic yield stress ratio for high tensile steel

The second interpretation of the apparent increased capacity for the wave period scenarios is that the strain rate model with the Cowper-Symonds parameters proposed by Paik is correct, and thus this increased capacity is real, although the industry practice is to neglect it. In this case it would not be consistent to consider the whole capacity increase for whipping scenarios, and the logic is to only retain the whipping increase relative to the wave one:  $\overline{f_{WWR}}$ .

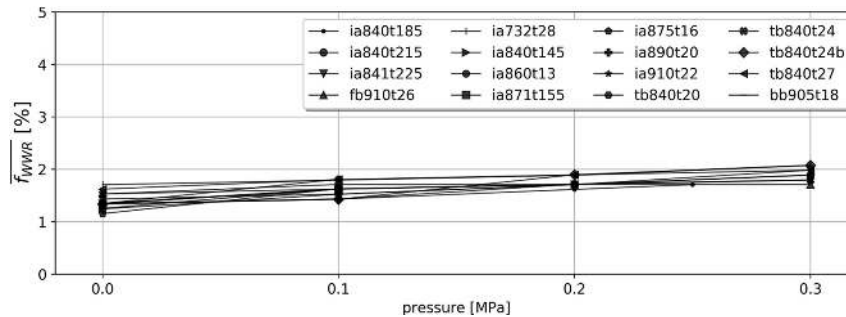


Fig. 14. Dynamic load ratio between whipping and wave scenarios vs. lateral pressure

It is beyond the scope of this work to determine which interpretation is correct, and also to propose an alternative strain rate model or set of coefficients. Therefore we decided to keep for now the parameters given by Paik and to consider the relative increase  $\overline{f_{WWR}}$  as the proper estimator of the increased capacity that could be used when designing or checking the structure against whipping. In

this case, the increment of the stiffened panel capacity under whipping scenario is between 1.6% and 2.1% when a pressure is applied and between 1.2% and 1.7% without pressure, as shown in Fig 14.

## 5. Real loading scenarios

The objective of this research work is to analyze the influence of the dynamic effects on the ultimate strength of stiffened panels. In the previous chapter it was shown that the inertial effect is negligible for a load period between 1.6 s and 16 s. Also, by using simplified loading scenarios, it was demonstrated that the strain rate effect is already existent in the wave loads, and if the panel is subjected to high frequency transient loads the strain rate effect will slightly increase the ultimate capacity. In a real environment, the high frequency transient loads are always combined with low frequency loads. Therefore, it can be anticipated that the strain rates obtained in the simplified “whipping period” scenarios in which 100% of the load was varying at the whipping frequencies were overestimated, and so was the strain rate effect on the panels capacity. In order to obtain better estimation of the actual panel capacity increase in the context of whipping, a hydro-elastic analysis was performed on an ultra large container ship to determine more realistic whipping loading scenarios. The principal characteristics of the ULCS used in this study are presented in Table 10.

Table 10. Geometrical characteristics of ULCS

Length overall	340 m	Breadth moulded	42.8
Draught	14.8 m	Capacity	8500 TEU
Geometric area of cross-section	6.55 m <sup>2</sup>	Position of neutral axis	12 m
Moment of inertia /Gy axis	707.5 m <sup>4</sup>	Moment of inertia /Gz axis	1958.22 m <sup>4</sup>
Shear centre transversal coordinate	-13.86 m	Warping moment of inertia	186144.6 m <sup>6</sup>
1 <sup>st</sup> vertical mode frequency	0.492 Hz	2 <sup>nd</sup> vertical mode frequency	1.036 Hz

The software HOMER, developed at Bureau Veritas, was used to perform the hydro-elastic coupling between the 3D hydrodynamic solver and a beam model based on non-uniform Timoshenko beam theory for the hull girder. The hydro-elastic model is based on the generalized modes approach; the complete procedure for the fully coupled seakeeping, slamming and whipping analysis can be found in Derbanne et al. (2010). First the mode shapes for several elastic modes are calculated and used later to extend the motion/ deformation modes in the hydrodynamic solver. After solving the hydrodynamic boundary value problems, the resulting pressure is integrated over the wetted surface in order to obtain the hydrodynamic forces, so that the coupled dynamic equation can be written:

$$\{-\omega_e^2([m] + [A]) - i\omega_e[B] + [k] + [C]\}\{\xi\} = \{F^{DI}\} \quad (9)$$

The solution of Eq. 9 gives the motion amplitudes and phase angles for 6 rigid body modes and a certain number of elastic modes. The non-linear time domain model uses the frequency domain hydrodynamic solution and transfers it to time domain using the inverse Fourier transform. In this way the following time domain motion equation is obtained:

$$([m] + [A^\infty])\{\ddot{\xi}(t)\} + [k]\{\xi(t)\} + \int_0^t [K(t - \tau)]\{\dot{\xi}(\tau)\}d\tau = \{F^{DI}(t)\} + \{Q(t)\} \quad (10)$$

The time domain calculation will automatically include the linear and non-linear springing. In order to calculate the slamming induced whipping response, the slamming forces, denoted by  $\{Q(t)\}$ , are calculated using the Generalized Wagner Model, and are added to the right hand term of Eq. 10.

The objective of the hydro-elastic analysis is to estimate the levels of different load components for the vertical bending moment and to determine the load time series which will be used to define real loading scenarios on the stiffened panels. The time domain simulations are performed on irregular waves using an increased design sea state (IDSS). Additional details about the IDSS methodology can be found in Derbanne et al. (2012). Fig. 15 shows a representative time variation of vertical wave bending moment (VWBM) at midship with and without slamming induced whipping.

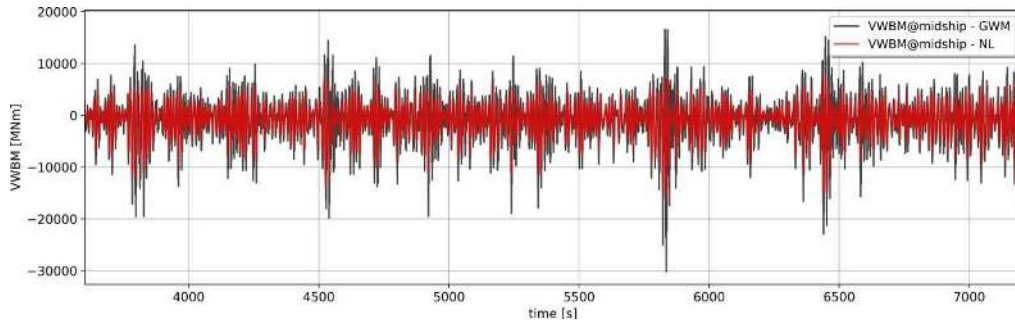


Fig. 15. Load time series for VWBM, with and without whipping, at midship

Based on the load time series several significant time samples are extracted and these loads are applied on the stiffened panel model. On a first step the lateral pressure loads are defined using a smooth step amplitude function. In the second step the axial compression due to vertical wave bending moment (with and without whipping) is applied. For each real loading scenario, shown in Fig. 16, the dynamic ultimate strength is computed using the procedure described in section 3. The results for the *wave* and *wave+whipping* real scenarios are presented in Table 11.

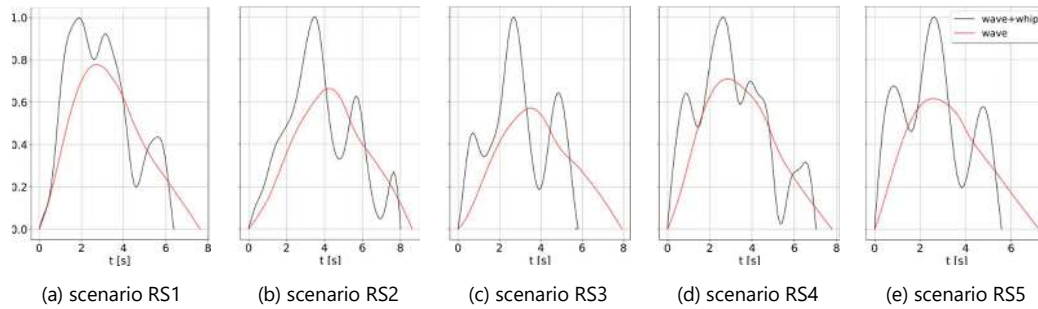


Fig. 16. Amplitude functions for real load time series extracted from time-domain hydro elastic analysis

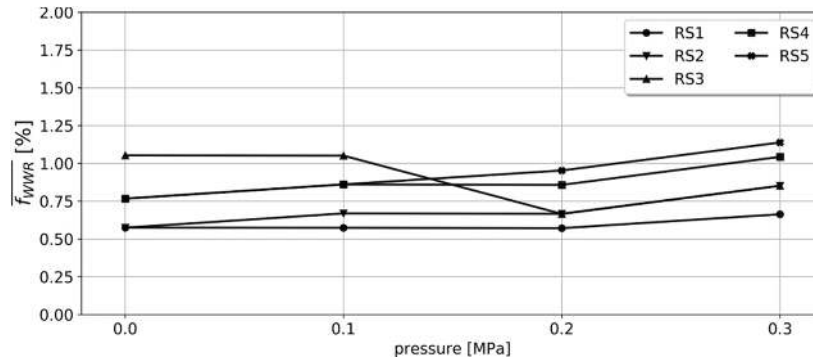


Fig. 17. Dynamic load factor ratio between *wave+whipping* and *wave* real scenarios for model *ia910t22*

The numerical results presented in Table 11 and Fig 17 are showing that the strain rate effect is already existent in the *wave* loads, and if the panel is subjected to *wave+whipping* loads the strain rate will increase. Due to higher strain rate the panel's capacity is increased by 0.4% to 1.3%. In a realistic loading scenario, the low frequency loads are combined with the high frequency loads; and therefore, it can be concluded that the simplified whipping scenario, defined in section 4, over predicts the increase of dynamic load factors due to whipping.

The whipping-wave dynamic load ratios obtained for pure axial compression (i.e. without lateral pressure) for the real loading scenarios are compared to the results obtained for simplified scenarios in Fig. 18. It can be observed that real loading scenarios lead to a significantly smaller ratio.



Table 11. Dynamic load factors [%] variation for real loading scenarios

case	prs	RS1		RS2		RS3		RS4		RS5	
		$\bar{f}_{d\_whip}$	$\bar{f}_{WWR}$	$\bar{f}_{d\_whip}$	$\bar{f}_{WWR}$	$\bar{f}_{d\_whip}$	$\bar{f}_{WWR}$	$\bar{f}_{d\_whip}$	$\bar{f}_{WWR}$	$\bar{f}_{d\_whip}$	$\bar{f}_{WWR}$
ia732t28	0.00	5.60	0.57	5.80	0.76	5.90	0.86	5.80	0.86	5.90	0.95
	0.30	6.50	0.76	6.70	0.95	7.20	1.32	6.80	1.14	6.80	1.14
ia840t145	0.00	3.70	0.39	3.80	0.39	4.00	0.58	4.00	0.68	3.90	0.58
	0.15	5.20	0.57	5.30	0.57	5.50	0.76	5.40	0.76	5.60	0.96
ia840t185	0.00	4.50	0.48	4.60	0.58	5.00	0.86	4.70	0.77	4.70	0.77
	0.25	5.70	0.57	6.00	0.76	6.00	0.76	6.00	0.86	6.10	0.95
ia841t225	0.00	4.90	0.58	5.00	0.57	5.50	1.05	5.10	0.77	5.10	0.77
	0.30	6.20	0.66	6.50	0.85	6.50	0.85	6.50	1.04	6.60	1.14
ia910t22	0.00	4.60	0.48	4.70	0.48	4.70	0.48	4.80	0.67	4.90	0.77
	0.30	5.80	0.57	5.90	0.67	6.10	0.76	6.10	0.95	6.20	1.05
ia840t27	0.00	5.10	0.48	5.30	0.67	5.70	1.05	5.40	0.86	5.40	0.86
	0.30	6.30	0.66	6.50	0.76	7.00	1.23	6.70	1.14	6.80	1.23

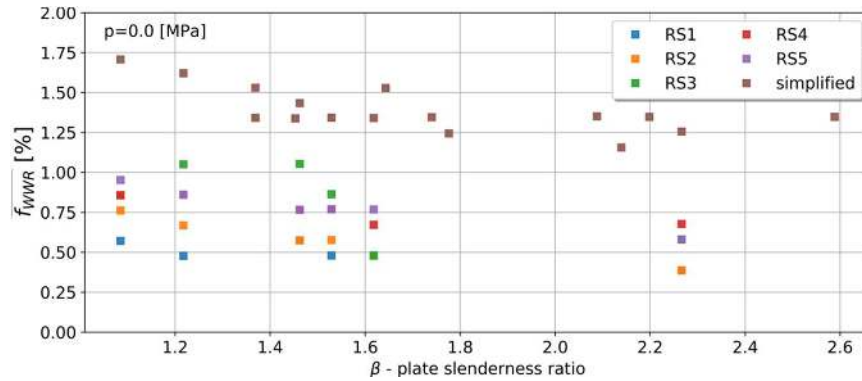


Fig. 18. Comparison of whipping-wave load ratio between simplified and real scenarios

## 6. Conclusion

In this paper, the numerical results of the dynamic collapse analysis for different stiffened panels, extracted from sixteen container ships, are presented. Each panel is subjected to in-plane biaxial loads and lateral loads associated with water pressure. In the first part of the analysis, the quasi-static capacity of these panels was determined. In the second part, the quasi-static capacity was used to define dynamic load time scenarios for two typical loading periods associated to *wave* and *whipping*. A new and proper definition of the panel dynamic ultimate capacity was introduced. By analyzing the numerical results, it can be concluded that the inertial effect on the ultimate capacity of stiffened panels is negligible for a periodic load varying from 1.6 to 16 s. On the other hand, the strain rate effect on the material constitutive law has some impact on the panel ultimate strength. With the new consistent definition of the dynamic capacity, the capacity increase originally in a [8.8% - 10.5%] range is reduced to [4.8 - 7.2 %].

However, under the hypotheses on the strain rate effect on the material flow stress that have been considered, the increase in ultimate capacity for wave loadings is already in the range of 3.5-6% while the industry practice is to consider no strain rate effect for such loads. The question whether this capacity increase for wave loads is real or is a bias due to the hypotheses is still open, but this result lead us to the conclusion that the capacity increase for *whipping period* scenarios has to be considered relatively to the increase for the wave period scenarios. When this is taken into account, the stiffened panel capacity increase under simplified *whipping period* scenario is only 1.2% to 2.1%.

The objective of the last part of the current research work was to compare the strain rate effect on the stiffened panel dynamic capacity under a real loading scenario, obtained from a hydro elastic analysis on a ULCS. The numerical results obtained from nonlinear finite element analyses are

showing that under a real *wave+whipping* loading scenario the stiffened panel's capacity is increased by 0.4% to maximum 1.3% comparing to a real *wave* loading scenario. It shows that simplified scenarios tend to over-predict the increase of the panel's capacity due to whipping.

Fig. 19 summarizes all the results presented in this paper. It shows that by over-increasing the applied load, as per Jiang's definition, the dynamic capacity was wrongly predicted. However, using an improved definition, the dynamic load factors are significantly reduced. Furthermore, considering that the wave scenario is accepted as quasi-static, the increase due to whipping is only between 1.2% and 2.1%. Moreover, the use of realistic loading scenarios further reduces the increase of the capacity with a factor of two. Therefore, it seems that the usual assumption that strain rate effect can be neglected in the ultimate strength analysis of ship structure subjected to wave loads can be extended to the analysis of structures subjected to whipping loads.

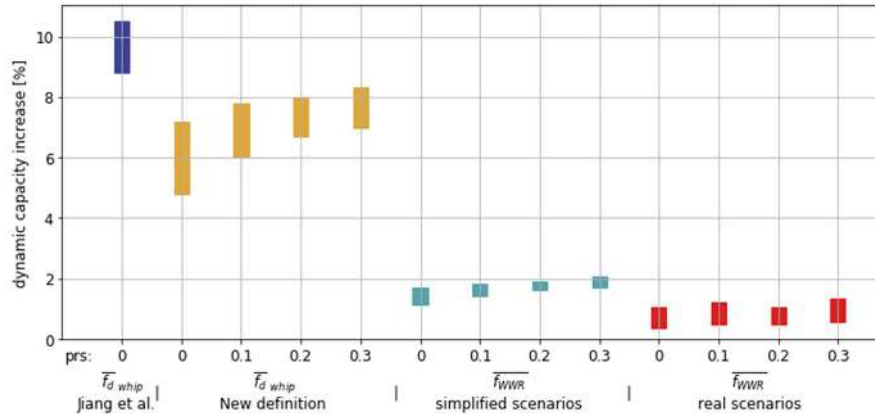


Fig. 19. Summary of dynamic capacity increase

In addition, according to several reports on the ultimate strength analysis of ULCS (Matsumoto et al. 2016, Fujikubo and Tatsumi 2017), at the point where the ultimate capacity of the hull girder is reached very few structural members undergo plastic deformations. Since the rest of the structure remains elastic, the strain rate effect on the hull girder ultimate bending strength of ULCS should be significantly smaller than the one on a single stiffened panel. Therefore, in a future work an extended ship model will be used to verify that the strain rate effect on the ultimate hull girder capacity of a container ship under whipping loads is practically negligible.

## Acknowledgements

The present research work was undertaken at École Centrale de Nantes, France, as a part of Ph.D. thesis on the analysis of whipping effects over the hull girder's ultimate strength. The first author is pleased to acknowledge the funding and support of Bureau Veritas via BV-ECN cooperation.

## References

- ABAQUS (2017). Dassault Systemes Simulia Corp, Johnston, RI, USA.
- Amlashi, H. K. and Moan, T. (2008). Ultimate strength analysis of a bulk carrier hull girder under alternate hold loading condition—a case study: Part 1: Nonlinear finite element modelling and ultimate hull girder capacity. *Marine Structures*, 21(4):327–352.
- Andersen, I. M. V. and Jensen, J. J. (2014). Measurements in a container ship of wave-induced hull girder stresses in excess of design values. *Marine Structures*, 37:54–85.
- Bishop, R. E. D. and Price, W. G. (1979). *Hydroelasticity of ships*. Cambridge University Press.
- Branch, M. A. I. (2008). Report on the investigation of the structural failure of MSC Napoli, English channel on 18 January 2007. Technical report, Marine Accident Investigation Branch.
- Bureau Veritas (2018). Rules on Materials and Welding for the Classification of Marine Units.
- Caldwell JB. 1965. Ultimate longitudinal strength. *Trans. Royal Institution of Naval Architects*. 107: 411-418.
- Choung, J., Nam, W., and Lee, J.-Y. (2013). Dynamic hardening behaviors of various marine structural steels considering dependencies on strain rate and temperature. *Marine Structures*, 32:49–67.
- ClassNK (2014). Investigation report on structural safety of large container ships. Technical report.

- Cowper, G. R. and Symonds, P. S. (1957). Strain-hardening and strain-rate effects in the impact loading of cantilever beams. Technical report, Brown Univ Providence Ri.
- Derbanne, Q., Bigot, F., and de Hauteclouque, G. (2012). Comparison of design wave approach and short term approach with increased wave height in the evaluation of whipping induced bending moment. *International Conference on Ocean, Offshore and Arctic Engineering*, pages 299–308.
- Derbanne, Q., Malenica, Š., Tuitman, J., Bigot, F., and Chen, X. (2010). Validation of the global hydroelastic model for springing & whipping of ships. *International Symposium on Practical Design of Ships and Other Floating Structures*, Rio de Janeiro, 331-340.
- Det Norske Veritas (2018). OS-B101 Metallic-Materials.
- Domnisoru, L. and Domnisoru, D. (1998). The unified analysis of springing and whipping phenomena. *Transactions of the Royal Institution of Naval Architects*, London, 140:19–36.
- Euler, L. (1759). Sur la force des colonnes. *Memoires de L’Academie des Sciences et Belles-Lettres*, 13:252–282.
- Fujikubo, M. and Tatsumi, A. (2017). Progressive collapse analysis of a container ship under combined longitudinal bending moment and bottom local loads. *Proceedings of the 6<sup>th</sup> International Conference On Marine Structures*, pages 235-242.
- ISO, EN (2009). 6892-1. Metallic materials-tensile testing-part 1: Method of test at room temperature. International Organization for Standardization.
- Jiang, L., Zhang, S., and White, N. (2012). Nonlinear finite element dynamic collapse analyses of stiffened panels. *Proceedings of the Sixth International Conference on Hydroelasticity in Marine Technology*, Tokyo, Japan, Sept, pages 19–21.
- Jones, N. (2011). *Structural impact*. Cambridge University Press.
- Khedmati, M. R., Zareei, M. R., and Rigo, P. (2010). Empirical formulations for estimation of ultimate strength of continuous stiffened aluminum plates under combined in-plane compression and lateral pressure. *Thin-Walled Structures*, 48(3):274–289.
- Kirchoff, G. (1850). Uber das gleichgewicht und die bewegung einer elastischen scheinbe. *Journal für die reine und angewandte Mathematik (Crelle’s Journal)*, 40:51–88.
- Lin, Y. (1985). *Structural longitudinal ship modelling*. PhD thesis, Department of Naval Architecture and Ocean Engineering, University of Glasgow Scotland.
- Manjoine, M. (1945). Influence of rate of strain and temperature on yield stresses of mild steel. *Journal of Applied Mechanics-Transactions of the ASME*, 12(3):A186–A186.
- Matsumoto, T., Shigemitsu, T., Kidogawa, M., Ishibashi, K., and Sugimoto, K. (2016). Examination of effect of lateral loads on the hull girder ultimate strength of large container ships. In *ASME 2016 35th International Conference on Ocean, Offshore and Arctic Engineering*. American Society of Mechanical Engineers.
- Paik, J. and Chung, J. (1999). A basic study on static and dynamic crushing behavior of a stiffened tube. *KSAE Trans.*, 1:219–238.
- Paik, J. K. (2018). *Ultimate limit state design of steel-plated structures*. John Wiley & Sons, 2nd edition.
- Paik, J. K. and Kim, B. J. (2002). Ultimate strength formulations for stiffened panels under combined axial load, in-plane bending and lateral pressure: a benchmark study. *Thin-Walled Structures*, 40(1):45–83.
- Paik, J. K., Kim, K. J., Lee, J. H., Jung, B. G., and Kim, S. J. (2017). Test database of the mechanical properties of mild, high-tensile and stainless steel and aluminum alloy associated with cold temperatures and strain rates. *Ships and Offshore Structures*, 12(sup1):S230–S256.
- Paik, J. K. and Seo, J. K. (2009a). Nonlinear finite element method models for ultimate strength analysis of steel stiffened-plate structures under combined biaxial compression and lateral pressure actions-part i: Plate elements. *Thin-Walled Structures*, 47(8-9):1008–1017.
- Paik, J. K. and Seo, J. K. (2009b). Nonlinear finite element method models for ultimate strength analysis of steel stiffened-plate structures under combined biaxial compression and lateral pressure actions-part ii: Stiffened panels. *Thin-Walled Structures*, 47(8):998 – 1007.
- Rolfé, S. T., Rhea, D. M., and Kuzmanovic, B. O. (1974). *Fracture-control guidelines for welded steel ship hulls*. Technical report, Kansas University Lawrence.
- Seng, S. (2012). *Slamming and whipping analysis of ships*. PhD thesis, DTU Mechanical Engineering.
- Shu, Z. and Moan, T. (2012). Ultimate hull girder strength of a bulk carrier under combined global and local loads in the hogging and alternate hold loading condition using nonlinear finite element analysis. *Journal of marine science and technology*, 17(1):94–113.
- Smith, C., Davidson, P., and Chapman, J. (1988). *Strength and stiffness of ships’ plating under in-plane compression and tension*. Royal Institution of Naval Architects Transactions, 130.
- Smith, C. S. (1977). Influence of local compressive failure on ultimate longitudinal strength of a ship’s hull. *Proc. Int. Sym. on Practical Design in Shipbuilding*, pages 73–79.
- Soreide, T., Moan, T., and Nordsve, N. (1978). On the behavior and design of stiffened plates in ultimate limit state. *Journal of Ship Research*, 22(4).
- Tuitman, J. and Malenica, Š. (2009). Fully coupled seakeeping, slamming, and whipping calculations. *Proceedings of the Institution of Mechanical Engineers, Part M: Journal of Engineering for the Maritime Environment*, 223(3):439–456.
- Turner, M. (1956). Stiffness and deflection analysis of complex structures. *Journal of the Aeronautical Sciences*, 23(9):805–823.
- von Karman, T. (1910). Untersuchungen über knickfestigkeit. In *Mitteilungen über orschungsarbeiten auf dem Gebiete des Ingenieurwesens insbesondere aus den Laboratorien der technischen Hochschulen*, pages 1–44. Springer.
- Zhang, S. (2016). A review and study on ultimate strength of steel plates and stiffened panels in axial compression. *Ships and Offshore Structures*, 11(1):81–91.
- Zhang, S. and Jiang, L. (2014). A procedure for non-linear structural collapse analysis. *International Conference on Ocean, Offshore and Arctic Engineering*, pages 19–21.